Letter

# Generation of fate patterns via intercellular forces

Hayden Nunley [1,*,†], Xufeng Xue [2,‡], Jianping Fu [2,3,4] and David K. Lubensky [1,5,§]

[1]Department of Biophysics, University of Michigan, Ann Arbor, Michigan 48109-1055, USA
[2]Department of Mechanical Engineering, University of Michigan, Ann Arbor, Michigan 48109-2125, USA
[3]Department of Biomedical Engineering, University of Michigan, Ann Arbor, Michigan 48109-2099, USA
[4]Department of Cell and Developmental Biology, University of Michigan Medical School, Ann Arbor, Michigan 48109-2200, USA
[5]Department of Physics, University of Michigan, Ann Arbor, Michigan 48109-1040, USA

(Received 30 April 2021; accepted 15 April 2025; published 4 June 2025)

Studies of fate patterning during development typically emphasize cell-cell communication via diffusible chemical signals. Recent experiments on stem cell colonies, however, suggest that in some cases mechanical stresses, rather than secreted chemicals, enable long-ranged cell-cell interactions that specify positional information and pattern cell fates. These findings inspire a model of mechanical patterning: fate affects cell contractility, and pressure in the cell layer biases fate. Cells at the colony edge, more contractile than cells at the center, seed a pattern that propagates via force transmission. Strikingly, our model implies that the width of the outer fate domain varies nonmonotonically with substrate stiffness, a prediction that we confirm experimentally; we argue that a similar dependence on substrate stiffness can be achieved by a chemical morphogen only if strong constraints on the signaling pathway's mechanobiology are met. Our findings thus support the idea that mechanical stress can mediate patterning in the complete absence of chemical morphogens, even in nonmotile cell layers, thus expanding the repertoire of possible roles for mechanical signals in development and morphogenesis. Future tests of additional model predictions, like the effect of anisotropic substrate rigidity, will further broaden the range of achievable fate patterns.

DOI: 10.1103/PhysRevResearch.7.L022051

Embryonic development depends on the differentiation of initially equivalent cells into spatial patterns of fates [1–12]. Such pattern formation often relies on diffusible chemical signals, called morphogens, for communication between cells. In one textbook scenario, localized morphogen secretion followed by diffusion and degradation creates a concentration profile that decays away from the source with a length scale determined by the diffusion coefficient and degradation rate. This exponential profile then conveys positional information to a field of cells that determine their fates by comparing the local morphogen level to internally specified thresholds [13]. More recently, it has become apparent that mechanical effects can also influence cell fate, but they have primarily been proposed to generate patterns by interacting with diffusible chemicals [14–18] or to take on entirely distinct roles, e.g., by conveying the rate of tissue flow during morphogenesis [19]. Here, inspired by recent experiments on stem cell colonies, we argue that mechanical stress can also entirely replace a chemical morphogen, specifying fate in a position-dependent manner in the absence of any diffusible chemical signals. In our mathematical model, cell fate biases contractility, and the resulting stresses bias fate. Strikingly, this model predicts a characteristic nonmonotonic dependence of fate pattern on substrate stiffness that we observe experimentally.

Evidence that the mechanical environment can affect stem cell differentiation in culture dates back at least to [20], which shows that isolated cells can measure the stiffness of their surroundings and use that information to autonomously bias their eventual fate. Subsequent work has argued that mechanical stresses can work together with chemical morphogens to set fate boundaries [14–18,21,22] and can couple to large-scale cell migration to allow fate patterns to emerge [23–26]. Several models have also been proposed wherein stress or strain feeds back on active contractility so as to create traveling waves of cell or tissue shape, without any intervening fate decision [27,28]. In contrast, here we are interested in a situation where diffusible chemical signals are absent and mechanical stress acts like a morphogen to convey positional information and fate cues between different individuals within a confluent cell layer.

This focus is motivated by an earlier report of fate patterning in stem cell colonies bound to micropatterned regions of an elastic substrate [29] [Figs. 1(b) and 1(c)]. In response to a spatially uniform supply of differentiation factors

*Contact author: nunley@umich.edu
†Present address: Center for Computational Biology, Flatiron Institute– Simons Foundation, New York, NY 10010, USA.
‡Present address: Center for Stem Cell & Organoid Medicine (CuSTOM), Cincinnati Childrens Hospital Medical Center, 3333 Burnet Avenue, Cincinnati, Ohio 45229-3026, USA.
§Contact author: dkluben@umich.edu

*Published by the American Physical Society under the terms of the Creative Commons Attribution 4.0 International license. Further distribution of this work must maintain attribution to the author(s) and the published article's title, journal citation, and DOI.*

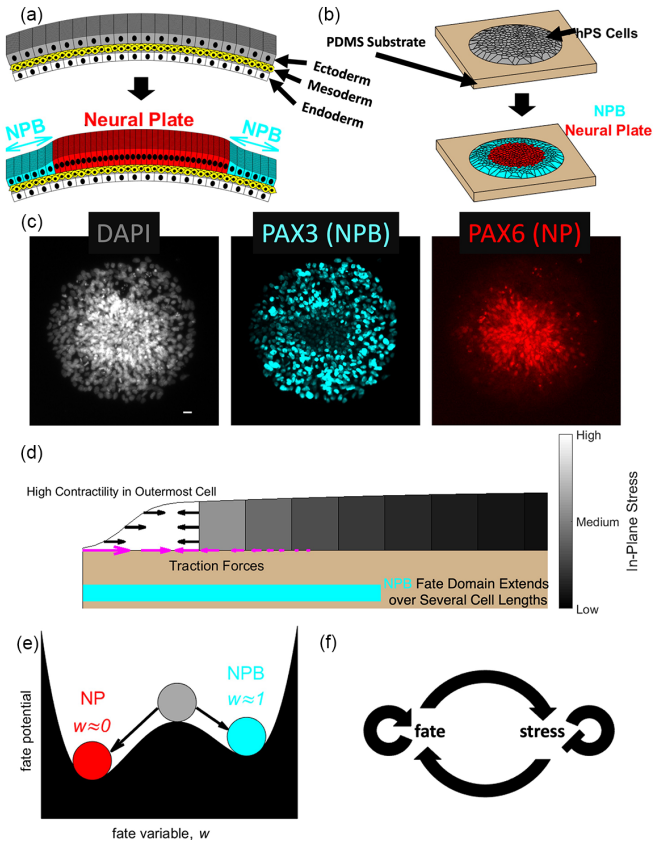



FIG. 1. (a) Neural induction *in vivo*. A strip of cells in the embryonic ectoderm differentiates into NP (red). Cells on either side form the NPB (cyan). (b) Neural induction *in vitro*. hPS cells bind to circular regions of elastic substrate (tan). Black lines: tessellations of nuclear positions before and after neural induction initiation. (c) Representative immunofluorescence images of hPS colony at day nine. DAPI counterstains nuclei. PAX3 and PAX6 label nuclei of NPB cells and NP cells, respectively. Scale bar, 20 μm; adapted from [29]. (d) Cell-cell communication via forces. Edge cells generate contractile forces (black arrows), and the resulting stresses bias cell fate. Importantly, cell-substrate traction forces (magenta) shape the spatial pattern of intercellular forces. Cyan indicates NPB domain, which extends inwards past the outermost, most contractile cell. (e) Schematic of differentiation from unstable state (gray) to stable cell state (red or cyan). (f) Feedback diagram for fate and mechanical stress for the mathematical model in Eqs. (1)–(4).

[11,29–32], cells differentiated into a binary fate pattern composed of neural plate (NP, colony center) or neural plate border (NPB, colony edge) fates [Fig. 1(c)]. (By contrast, the *in vivo* formation of these same fate domains [Fig. 1(a)], crucial to the development of the nervous system, is generally believed to rely on gradients of chemical signals secreted by a neighboring group of cells which are absent *in vitro* [10,33,34]). As we describe in more detail below, multiple lines of experimental evidence support the hypothesis that mechanical stress conveys fate information in this system: Most dramatically, blocking expression of signals (e.g., BMP4 and NOGGIN) known to be important for the NP/NPB fate decision *in vivo* had no effect on the *in vitro* pattern, while direct mechanical stretching of the cell layer strongly biased cell fate [29].

In the remainder of this Letter, after summarizing the evidence for mechanics-guided patterning in the experiments reported in [29], we propose a mathematical model [Figs. 1(d)–1(f)] for the formation of a fate pattern in response to mechanical stresses generated by the cell layer itself. We build on previous studies [35–37] by introducing feedbacks between mechanical stress and a bistable fate. These feedbacks lead to the spontaneous emergence of nonuniform patterns of cell fate and contractility. Notably, this pattern formation process cannot be understood in terms of a linear instability but instead relies on the boundary-driven nucleation and growth of fate domains. To explain the effects of different model parameters on the size of the outer (NPB) fate domain, we first derive an expression for this width in the analytically tractable limit of a quasi-1D cell layer bound to a very thin substrate; we then verify numerically that the same basic trends hold for the more experimentally relevant case of a cell layer atop a substrate of non-negligible thickness. Experimental tests verify key predictions of our model, most importantly that the NPB domain width depends nonmonotonically on substrate stiffness. We close with further model predictions and a discussion of the model's implications for the corresponding differentiation process *in vivo*.

*Experimental evidence for fate-stress feedback in vitro.* Fate patterning in stem cell colonies often relies on secretion of morphogens in the BMP family and their antagonist NOGGIN [38,39] and/or on localization of receptors for these morphogens that promotes differential activation near the colony border [39]. Xue *et al.*'s experiments exclude both possibilities in their system [29]. By contrast, if fate patterning depends on reciprocal coupling between fate and mechanical stress, one would expect that the two cell fates (NP, NPB) differ mechanically and that mechanical perturbations bias cell fate. Xue *et al.* tested the former prediction by measuring cell-substrate forces and the latter by mechanical stretching of colonies. In this section, we provide quantitative analyses of these previously published data [29].

Imaging of cell layers bound to micropost force sensors enabled the measurement of forces exerted by cells on their substrate. Each micropost's deflection is proportional to the force applied by the cell bound to it [Figs. 2(a)–2(d)] [29,36,40–43]. Xue *et al.* found that these forces are highest near the colony edge [29], as is expected even for cell layers of uniform mechanical properties [35,36]. Here, we analyze these data in more detail to test whether the cell layers have nonuniform mechanical properties: Fig. 2(c) shows average radial post deflection at a given distance from the colony center and a fit to a mechanical model based on [35,36] (additional examples in [40,44]). These fits reveal that the deflection profiles are not consistent with uniform cellular contractility but instead reflect the presence of three regions in the circular colonies: a noncontractile central region, corresponding roughly to the PAX6-expressing (NP) domain, surrounded by two annular, contractile regions that together coincide with the PAX3-expressing (NPB) domain. The next section proposes an explanation for the presence of two distinct NPB regions of differing contractility [44].

To determine whether mechanical perturbations can bias fate, Xue *et al.* then stretched the colony central region during differentiation [29] and found that all cells then tend to

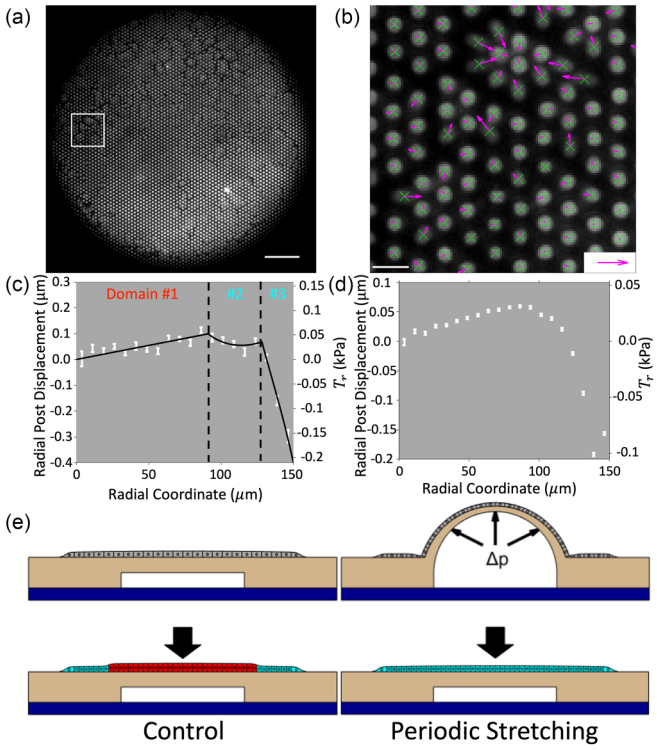



FIG. 2. (a) Example of contrast-enhanced image of microposts under cell colony, two days after neural induction initiation [40]. Scale bar, 40 μm. (b) Posts from white box in (a). Cells exert forces (magenta arrows) on posts. Green X: detected post positions. Scale bar: 5.0 μm. Scale arrow (bottom right): 15 nN. (c) Concentrically averaged radial post displacements versus radial coordinate, for the colony in (a). Average traction stress $T_r$ between cell and substrate (proportional to post displacement) is also indicated. Black line: three-domain fit [40,44]. We interpret the outermost region as a ring of spread, highly contractile cells at the colony edge, the intermediate region as a contractile ring of bulk cells, and the inner region as noncontractile cells. Dashed lines: boundaries between domains in fit. Red and cyan labels: hypothesized relationship between these domains and NP and NPB fates, respectively. (d) Post displacement profiles averaged over $n = 42$ colonies. Since the elbowlike feature's position [see (c)] shifts from sample to sample, this feature smooths out on average. (e) Left: Control experiments show differentiation into NP (red) and NPB (cyan) domains. Right: Stretching the colony's center via a microfluidic chamber causes central cells to become NPB. (a), (b), (e) adapted from [29].

adopt the NPB fate [Fig. 2(e)]; similarly, when constrained to larger areas, single cells more often show prominent nuclear p-SMAD 1/5, another marker of NPB fate [29]. Thus, NPB cells are more contractile than NP cells, and stretching biases cells to the NPB fate.

*Minimal model of mechanical fate patterning.* Motivated by the experiments in [29], we develop a minimal model for a binary fate decision coupled to mechanical stress. We map fate to a single, phenomenological variable $w$ evolving in a bistable potential with minima corresponding to NP ($w \approx 0$) and NPB ($w \approx 1$) [Fig. 1(e)]; similar mappings have proven useful in describing other fate transitions [45,46]. Though $w$ does not correspond narrowly to the concentration of one particular factor, its pattern reflects those of relevant fate marker(s) coupled to a mechanosensitive signaling pathway [44].

We then introduce minimal couplings between $w$ and the cell layer's two-dimensional in-plane stress tensor $\underline{\underline{\sigma}}$ [Eqs. (1)–(4) below]: Mechanical pressure $[-\mathrm{tr}(\underline{\underline{\sigma}})]$ linearly biases $w$, and active stress ($\sigma_a$) is proportional to $w$.

The coupling from stress to fate, together with fate bistability, leads to the dynamics for $w$ :

$$\tau_w \frac{\partial w}{\partial t} = f(w, \mathrm{tr}(\underline{\underline{\sigma}})) + D\tau_w \nabla^2 w, \tag{1}$$

$$f(w, \mathrm{tr}(\underline{\underline{\sigma}})) = w(w - w_{\mathrm{mid}})(1 - w) + \alpha(\mathrm{tr}(\underline{\underline{\sigma}}) - \sigma^*). \tag{2}$$

Here $\alpha > 0$ is a constant. $\tau_w$ is the time scale of fate evolution, and $w_{\mathrm{mid}}$ sets the asymmetry of the potential in the absence of stress feedback [Fig. 1(e)]. The constant stress offset $\sigma^*$ strongly influences the NPB domain's width. The diffusion term in Eq. (1) is introduced to regularize spatial variation of $w$ at short scales; $\sqrt{D\tau_w}$ determines the width of the wall separating the NP and the NPB. To avoid driving patterning in a stress-independent manner, we assume no-flux boundary conditions on $w$ at the colony edge.

To complete our model, we must also specify how a fate pattern $w$ generates a pattern of active stress and thus a cell layer stress field $\underline{\underline{\sigma}}$. We initially assume that the cell layer is elastic on the timescale of differentiation, thin relative to its lateral extent, and rests on a very thin substrate that effectively acts like an array of uncoupled, Hookean springs. In that case, force balance requires that $\mathrm{div}\,\underline{\underline{\sigma}} \propto \vec{u}$, where $\vec{u}$ is the substrate displacement [35,36]. Although we simulate the model for more experimentally relevant geometries and substrate thicknesses in Figs. 3 and 4 (equations in [44]), in this section and the next we focus on the case of a cell layer in a simple stripe geometry where one can derive analytic expressions for the NPB domain width. The stripe is infinite along the $y$ axis and is symmetric about the center ($x = 0$). Exploiting this symmetry, we assume in what follows, without loss of generality, that $x \geqslant 0$. The stripe has zero-stress boundary conditions at its edge at $x = x_0$. $\mathrm{div}\,\underline{\underline{\sigma}} \propto \vec{u}$ then simplifies to (derivation in [36])

$$0 = l_l^2 \frac{d^2\sigma_{xx}}{dx^2} - \sigma_{xx} + \frac{\sigma_a(x)}{2}, \tag{3}$$

$$\sigma_a(x) = -\frac{h_c B_c}{(1-\nu)} \tilde{P} w(x). \tag{4}$$

Here $h_c$, $B_c$, and $\nu$ are the cell layer height, modulus, and Poisson's ratio, respectively. The minimal coupling from fate to stress is implemented by an active stress $\sigma_a$ that is proportional to the preferred strain $\tilde{P} < 0$ and to the fate variable $w$, so that active stresses are generated primarily by NPB ($w \approx 1$). In this geometry, the cell layer does not contract along the $y$ direction, so $\sigma_{yy} = \frac{\sigma_a(x)}{2}$ everywhere. The localization length $l_l$ sets the length scale over which $\sigma_{xx}$ varies along the $x$ direction. The ratio of cell layer stiffness to substrate stiffness determines $l_l$, with $l_l$ decreasing as the substrate becomes stiffer [35,36].

In our system, the fate-stress couplings inferred from experiments are of common sign [Fig. 1(f) and Eqs. (1)–(4)] and are thus incompatible with Turing-like, linear instabilities [5,47], by which patterns might arise spontaneously from

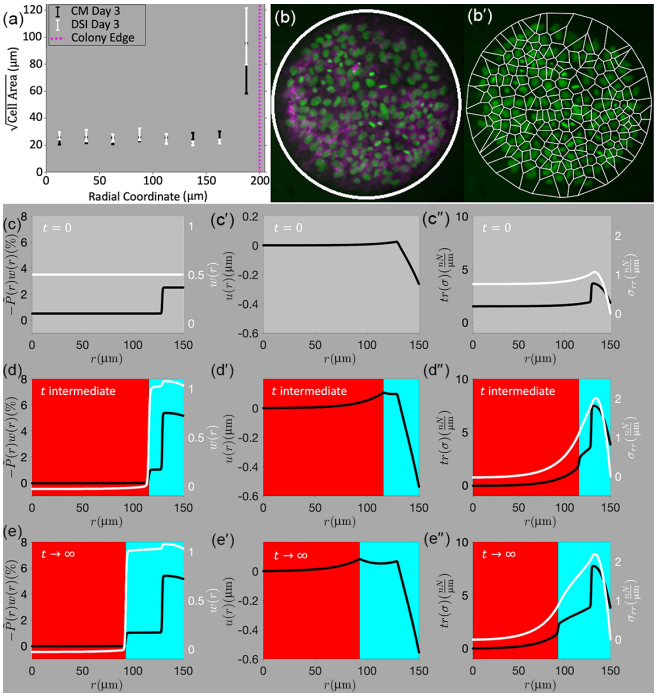



FIG. 3. (a) Square root of cell area versus radial coordinate. In neural induction medium (DSI) and in conditioned medium (CM), cell area is largest near the colony edge (magenta line). (b) Colony, immunostained for DAPI (green) and E-Cad (magenta), at day three in DSI. White circle: micropatterned colony edge. Data in [50]. (b′) Colony from (b) showing Voronoi tessellation based on nuclear positions. Colony diameter, 400 μm. (c)–(e″): Initial condition (c)–(c″), intermediate state (d)–(d″), and fixed point (e)–(e″) for the model on a thin substrate or microposts in a disk geometry [Eqs. (1) and (2) for $w$ and the generalization of Eqs. (3)–(5) for $\underline{\underline{\sigma}}$ in a disk; full equations in [44]). All parameters except for $\alpha$, $w_{\rm mid}$ , and $\sigma^*$ (Table S6 and accompanying text [44]) are from a fit to micropost data in Figs. 2(a)–2(c). We plot the fate variable $w(r)$ and negative target strain $-\tilde{P}w$ (left), post displacement (center), and mechanical stresses in the cell layer (right) [51]. Initially, $w$ is uniform. At some intermediate time, $w \approx 1$ in the region near the colony edge [cyan background, (d)–(e″)]. These cells generate stress in their neighbors, and the fate boundary (between cyan and red) moves inward until stress at the fate boundary reaches the coexistence stress.

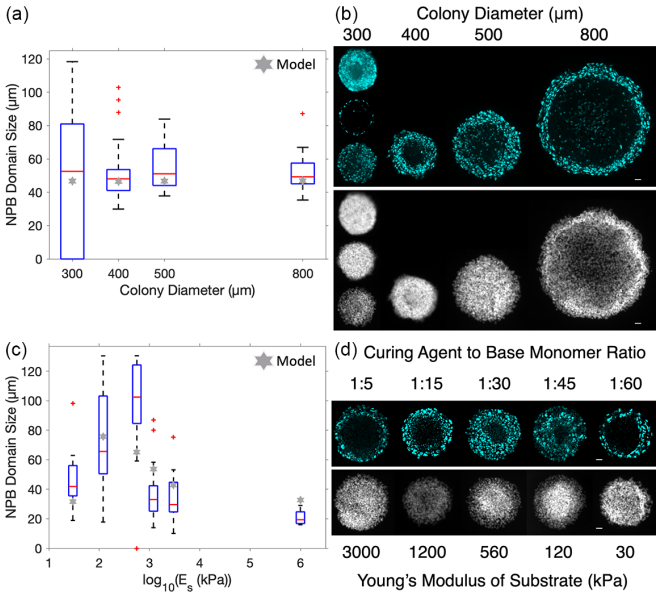



FIG. 4. (a) NPB domain size, as estimated by PAX3 staining, versus colony diameter. The median width of the NPB domain (red lines; blue boxes give 25th and 75th percentile, respectively) is approximately independent of colony diameter. Red points: outliers. (b) Examples of colonies immunostained for PAX3 (cyan) and DAPI (gray). Experimental data in (a) and (b) from [29,56]. (c) NPB domain size versus the logarithm of substrate's Young's modulus $E_s$, showing nonmonotonic dependence at fixed colony diameter (400 μm). By changing the curing agent to base monomer ratio used in preparing the PDMS substrate, we alter its stiffness over orders of magnitude. The substrate thickness varies more mildly with the same ratio (40 μm, 81 μm, 101 μm, 120 μm, 134 μm for 1:5, 1:15, 1:30, 1:45, 1:60). We account for this effect as well as the change in stiffness in our model calculations (stars), which employ a modification of Eqs. (3) and (4) that includes finite substrate thickness (see [44] for details and for the parameters used to optimize the fit between model and experimental data). The data point with the highest modulus is from a glass, not PDMS, substrate (glass colony conditions in Methods [44]). (d) Examples of cell colonies on PDMS immunostained for PAX3 (cyan) and DAPI (gray). Scale bars, 40 μm. See data in [56].

small fluctuations about a spatially uniform state. Instead, we hypothesize that mechanical signals from cells at the colony's edge drive the formation of the NPB. In related systems, cells near the colony edge are known to be more contractile [48,49]. Indeed, immunostaining of nuclei and adherens junctions during differentiation in our system reveals that edge cells spread to a larger area per cell than bulk (i.e., nonedge) cells [Figs. 3(a)–3(b′)] [50]. The edge cells coincide well with the outermost region of high contractility whose existence we inferred from micropost data (Fig. 2(c), [44]). To introduce more contractile edge cells, we allow the preferred strain to depend on position:

$$\tilde{P}(x) = \tilde{P}_1 + (\tilde{P}_2 - \tilde{P}_1)\Theta(x - (x_0 - \Delta x)) \,, \qquad (5)$$

where $\tilde{P}_2 < \tilde{P}_1 < 0$ are constants, $\Delta x$ is the width of the edge cells, and $\Theta$ is the Heaviside step function.

With this choice of $\tilde{P}(x)$, we find that the highly contractile cells at the colony edge generate stresses in neighboring cells that accordingly increase their $w$ and thus upregulate contractility. As the example simulation in Figs. 3(c)–3(e″) shows [51], the fate boundary separating the NP and NPB domains hence moves inward until the stress at the fate boundary equals a coexistence stress that (we show below) depends strongly on $\sigma^*$. In these simulations, all parameters are experimentally controlled ($x_0$ and substrate stiffness) or measured ($\Delta x$, $h_c B_c$, $\tilde{P}_1$, and $\tilde{P}_2$), except for four ($\sigma^*$, $\alpha$, $w_{\rm mid}$, and $\sqrt{D\tau_w}$). [For $\nu$, we make the reasonable assumption that the cell layer is nearly incompressible in 2D. Because $\nu$ appears only in products with other parameters in Eqs. (3) and (4), $\nu$ can moreover be viewed as rescaling our estimates of other parameters rather than as an independent parameter in its own right]. With $\sqrt{D\tau_w} \ll l_l$, as discussed in the next section, only three parameters are not constrained. For these parameters, we use all or a subset to fit the model to experimental data

(e.g., the data in Fig. 1(c) or in Fig. 4; details of fitting procedure in [44]). Notably, our phenomenological model, based on experimentally motivated assumptions and experimentally estimated parameters, reproduces measured traction forces between the cell layer and the substrate [compare Fig. 2(c) to Fig. 3(e′)]. In addition, the model predicts, and we have verified experimentally, that the fate boundary moves inward from the colony edge during differentiation (Figs. 3(d) and 3(e) and [44]). To better understand our numerical results, in the next section we derive an approximate analytic expression for the NPB domain width and explore its parameter dependence.

*NPB domain width in the domain wall limit.* Although the final NP-NPB pattern could, in principle, depend strongly on all the parameters listed above, one might hope that the width of the NPB domain is instead primarily sensitive to a few dimensionless combinations. To see that this is the case, we next analytically determine the fate boundary's position for a cell layer in a stripe geometry and in the "domain wall" limit, in which the fate boundary is much sharper than $l_l$ ($D\tau_w \ll l_l^2$) and matched asymptotic methods may be applied [44,52–54].

In outline, the calculation proceeds as follows: We assume that the pattern is symmetric about the colony center and consists of one central NP domain separated from an NPB domain on each side by a sharp domain wall. Away from these two fate boundaries, $w$ is slowly varying in the patterned steady state and we may set $D\tau_w \approx 0$, so that $w$ satisfies $f(w, \mathrm{tr}(\underline{\underline{\sigma}})) = 0$. The high and low roots of this equation correspond to the NPB and NP fates. Here, we make the further approximation that these roots depend only weakly on $\underline{\underline{\sigma}}$ and set $w \approx 1$ and $w \approx 0$ everywhere in the NPB and NP domains, respectively. Then, it only remains to find the location of the fate boundaries where $w$ changes rapidly from one to zero. A well-known result holds that a stationary front solution of Eqs. (1) and (2) connecting high and low $w$ is only possible at a single value of the stress, which satisfies an integral condition akin to the Maxwell construction for phase coexistence [54]. Assuming two fate boundaries positioned symmetrically at a distance $x_1$ from the colony center, we know $w$, and hence the active stress everywhere, so we can calculate the stress at the fate boundaries. We must then choose $x_1$ self-consistently so that the stress at the boundaries equals the unique allowed coexistence value.

One subtlety in our calculation arises from the tensorial nature of the stress. We require a stress field that changes only on the slow scale $l_l$ and does not jump sharply at the domain wall. Because $\sigma_{yy} = \frac{\sigma_a(x)}{2}$ varies rapidly across the wall, $\mathrm{tr}(\underline{\underline{\sigma}})$ does not meet this condition. Instead, we introduce the new field $\sigma_{\mathrm{smooth}} = \mathrm{tr}(\underline{\underline{\sigma}}) + \frac{h_c B_c \tilde{P} w}{2}$ that remains smooth near the domain wall and so can be approximated as constant on the scales over which $w$ changes [44]. As just described, we can then calculate the value $\sigma^{FB}_{\mathrm{smooth}}(x_1)$ of this field at the fate boundary as a function of the boundary position $x_1$. The correct position satisfies $\sigma^{FB}_{\mathrm{smooth}}(x_1) = \overline{\sigma^{FB}_{\mathrm{smooth}}}$, where $\overline{\sigma^{FB}_{\mathrm{smooth}}}$ is the allowed coexistence value of the smooth stress set by the integral condition. Notably, this equation does not have solutions $x_1$ for all parameter choices; in some parameter regimes, a pattern with coexisting NP and NPB domains is not possible. In particular, $\overline{\sigma^{FB}_{\mathrm{smooth}}}$ depends on $w_{\mathrm{mid}}$, $\alpha$, $h_c B_c \tilde{P}_1$ (because of the prefactor to the $w$ term in the definition of $\sigma_{\mathrm{smooth}}$), and, most strongly, $\sigma^*$; $\sigma^*$ must thus fall within a certain range for a stable pattern to occur.

In the experimentally relevant limit $l_l \ll x_0, x_1$, one can actually solve $\sigma^{FB}_{\mathrm{smooth}}(x_1) = \overline{\sigma^{FB}_{\mathrm{smooth}}}$ for $x_1$ to find the NPB domain width $x_0 - x_1$ [44]:

$$x_0 - x_1 = -l_l \log\left(a + \sqrt{-1 + a^2 + 2\overline{\sigma^{FB}_{\mathrm{smooth,ND}}}}\right), \quad (6)$$

where $a = \left(\frac{\tilde{P}_2}{\tilde{P}_1} + \left(1 - \frac{\tilde{P}_2}{\tilde{P}_1}\right)\cosh\left(\frac{\Delta x}{l_l}\right)\right)$ and $\overline{\sigma^{FB}_{\mathrm{smooth,ND}}} = \frac{2(1-\nu)}{h_c B_c(-\tilde{P}_1)(1+\nu)}\overline{\sigma^{FB}_{\mathrm{smooth}}}$. $\overline{\sigma^{FB}_{\mathrm{smooth,ND}}}$ is a nondimensionalized version of $\overline{\sigma^{FB}_{\mathrm{smooth}}}$. The condition for the existence of a stable NP-NPB patterned solution is $a \leqslant a + \sqrt{-1 + a^2 + 2\overline{\sigma^{FB}_{\mathrm{smooth,ND}}}} < e^{-\frac{\Delta x}{l_l}}$.

In the domain wall limit, the NPB domain size thus depends on one dimensionful quantity, $l_l$, and three dimensionless quantities, $\frac{\tilde{P}_2}{\tilde{P}_1}$, $\frac{\Delta x}{l_l}$, and $\overline{\sigma^{FB}_{\mathrm{smooth,ND}}}$. The nondimensionalized coexistence stress itself depends implicitly on other parameters, including $\alpha$, $w_{\mathrm{mid}}$, and $\sigma^*$, through the integral constraint discussed above.

Two model predictions are apparent from Eq. (6). First, the NPB domain width $x_0 - x_1$ is independent of the colony width $x_0$ in the limit $x_0 \gg l_l$. Second, the NPB domain width has a nontrivial—indeed nonmonotonic—dependence on the parameter $l_l$: Because of the appearance of the length scale ratio $\Delta x/l_l$ in the definition of $a$, it can be seen from inspection that $x_0 - x_1$ varies nonlinearly with $l_l$. In fact, one can show that the derivative of Eq. (6) with respect to $l_l$ is the sum of two $l_l$-dependent terms of differing signs. This generates an NPB domain width that depends nonmonotonically on $l_l$ and thus—because $l_l$ varies inversely with substrate stiffness—on substrate stiffness. Such behavior arises because, although the stress exerted by the contractile edge cells decays exponentially away from the edge on a lengthscale $l_l$ that decreases as the substrate becomes stiffer, the prefactor in front of this exponential decay increases along with substrate stiffness. In fact, the same competing effects can already be seen in the even simpler case of an infinite colony, where the solution of Eqs. (3) and (4) for a delta function active stress at the origin is $\sigma(x) \sim (1/l_l)\mathrm{e}^{-|x|/l_l}$. The finite colony size and no-stress boundary conditions in our problem lead to a more complicated functional form but do not change the basic idea. (A similar effect is also at the origin of a previous prediction that the force between cells in a monolayer can vary nonmonotonically with substrate stiffness [55]).

In the next section, we show numerically that both of these predictions still hold for more realistic geometries and substrate thicknesses, and we test them experimentally.

*NPB domain width does not depend on colony diameter, depends nonmonotonically on substrate stiffness.* We now turn our attention from analytically tractable limits to the general case of a differentiating cell layer on a finite-thickness substrate. To allow for direct comparison between predictions

and experiments, we simulate a mechanical model for finite-thickness substrates (based on [37]; equations in [44]) coupled to Eqs. (1) and (2) for $w$ [51].

We previously reported that the NPB domain width does not change significantly as the colony diameter varies from 300 to 800 μm [29,56] in experiments, and we saw the same behavior analytically in the previous section in certain limits [Eq. (6)]. Our full, numerical model recapitulates this insensitivity to colony diameter for diameters much larger than $l_l$ [Figs. 4(a) and 4(b)] and further predicts that the fate pattern is lost when the diameter becomes too small, consistent with experimental observations that patterning often fails for small diameters (300 μm) [44].

We next consider how the NPB domain width varies with substrate stiffness. In the thin substrate limit, the basic length scale $l_l$ grows as the substrate becomes softer, and one might expect that the NPB domain width would have the same simple dependence. We saw above, however, that additional factors dependent on $\Delta x/l_l$ are present and vary in the opposite direction, leading to the surprising conclusion that the domain width is a nonmonotonic function of $l_l$. Simulations of the model with a finite thickness substrate predict the same nonmonotonic dependence of NPB domain size on substrate stiffness in the more general case (Fig. 4(c), [51]).

Experiments confirm this prediction [Figs. 4(c) and 4(d)] [56]: As the substrate stiffness increases from 30 kPa to 3 MPa at a constant colony diameter of 400 μm, the NPB domain width increases from ≈40 μm to ≈100 μm before decreasing to ≈25 μm.

So far, we have focused on colonies grown in isotropic environments; however, our model also makes predictions for substrates of anisotropic stiffness, i.e., whose stiffness depends on the angle between the displacement and a fixed axis [57,58]. Simulations reveal that the NPB domain width then varies as a function of polar angle [44]. Similarly, even for substrates of isotropic stiffness, modulating the degree of edge cell spreading should make the resulting NPB domain width angle dependent. These two predictions, as well as others, are explored in [44,51] and await experimental tests.

*Discussion.* We have argued that, in some hPS cell systems, mechanical stress can act like a conventional morphogen, conveying positional information and patterning cell fates in a position-dependent, non-cell-autonomous manner even in the absence of any spatially varying chemical signals. In our experimentally motivated model, highly contractile cells at the edge of the colony act as a source of stress. To determine whether the local stress biases their fate to NP or to NPB, cells compare the local stress to $\sigma^*$, as in the textbook case of a chemical morphogen discussed above. Our model of a mechanical morphogen, however, goes beyond the simplest scenario for a chemical morphogen, because in the mechanical case the differentiating cells then generically modify the stress in the cell layer by changing their own contractility. This behavior represents an unexpected, new mode of pattern formation in living systems. As predicted by our model, we find experimentally that the width of the NPB fate domain in our colonies depends nonmonotonically on the substrate stiffness. The model also makes additional predictions, including for the shape of the fate pattern on substrates of anisotropic stiffness [44].

In contrast to a recent study [59] that also considered a fate pattern driven by feedback between contractility and stress, our model has couplings whose signs are inconsistent with a Turing-like linear instability. Patterning, in the form of a sharp domain boundary, instead propagates inwards from a contractile colony edge. Notably, micropost deflection measurements indicate that the in-plane mechanical stresses in our colonies are comparable to stresses that induce mechanotransduction responses in other systems [60].

Although the observed nonmonotonic dependence on substrate stiffness is a strong indication that our patterns have a mechanical origin, it is important to ask whether a conventional morphogen (perhaps a member of the WNT family [11]) could ever produce similar behavior. Morphogen concentrations can of course obey a screened diffusion equation like Eq. (3) (but with $\sigma_{xx}$ replaced by the morphogen concentration). Thus, if cells responded autonomously to changes in substrate stiffness by varying the diffusion length in exactly the right way, this could lead to behavior like that observed in Fig. 4(c). One obvious way for cell-autonomous changes to affect the diffusion length would be for rates of ligand internalization and degradation to depend on the substrate stiffness sensed by the cells [61]. Importantly, however, this dependence would have to be very strong to reproduce our experimental results; we estimate that the effective ligand degradation rate would need to vary by at least a factor of 100 over the range of stiffnesses tested [44]. Thus, although we cannot categorically rule out a nonmechanical origin for our observations, we can say that any signaling by a diffusible morphogen that mimicked the predictions of the mechanical model would have to obey strong and specific constraints.

Finally, it is worth emphasizing that, whereas chemical morphogens do not appear to play a role in our *in vitro* experiments, BMP proteins almost certainly are an important factor in the NP-NPB fate decision *in vivo* [62–64]. To fully understand the functional importance of the mechanical effects uncovered here, it will be necessary to tease out, via extensions of our model to include chemical biases, how mechanical morphogens interact with diffusible chemical signals *in vivo* to promote robust patterning and morphogenesis.

*Acknowledgments.* This work was supported by the National Science Foundation (CMMI 1917304 to J.F., DGE 1256260 to H.N., and DMR 2243624 to D.K.L.), by pilot project funding from the NSF-Simons Center for Quantitative Biology (Simons Foundation/SFARI 597491-RWC and the National Science Foundation 1764421 to J.F. and D.K.L.), and by the Michigan-Cambridge Collaboration Initiative (to J.F.). The computations reported in this paper were in part performed using resources made available by the Flatiron Institute.

*Data availability.* The data that support the findings of this article are openly available [40,50,51,56]. For Figs. 2 and 4, experimental data and corresponding code for analysis are in [40,56], respectively. For Figs. 3(a) and 3(b), experimental data and corresponding code for analysis are in [50]. Code for simulations in Figs. 3(c)–3(e″), 4(a), and 4(c) is in [51].

[1] C. J. Chan, C.-P. Heisenberg, and T. Hiiragi, Coordination of morphogenesis and cell-fate specification in development, Curr. Biol. **27**, R1024 (2017).

[2] W. Driever and C. Nüsslein-Volhard, The bicoid protein determines position in the Drosophila embryo in a concentration-dependent manner, Cell **54**, 95 (1988).

[3] T. Gregor, D. W. Tank, E. F. Wieschaus, and W. Bialek, Probing the limits to positional information, Cell **130**, 153 (2007).

[4] E. Hannezo and C.-P. Heisenberg, Mechanochemical feedback loops in development and disease, Cell **178**, 12 (2019).

[5] A. M. Turing, The chemical basis of morphogenesis. 1953, Bull. Math. Biol. **52**, 153 (1990).

[6] K. D. Gallagher, M. Mani, and R. W. Carthew, Emergence of a geometric pattern of cell fates from tissue-scale mechanics in the Drosophila eye, eLife **11**, e72806 (2022).

[7] D. K. Lubensky, M. W. Pennington, B. I. Shraiman, and N. E. Baker, A dynamical model of ommatidial crystal formation, Proc. Natl. Acad. Sci. USA **108**, 11145 (2011).

[8] F. Corson, L. Couturier, H. Rouault, K. Mazouni, and F. Schweisguth, Self-organized Notch dynamics generate stereotyped sensory organ patterns in Drosophila, Science **356**, eaai7407 (2017).

[9] M. Bauer, M. D. Petkova, T. Gregor, E. F. Wieschaus, and W. Bialek, Trading bits in the readout from a genetic network, Proc. Natl. Acad. Sci. USA **118**, e2109011118 (2021).

[10] C. D. Stern, Neural induction: Old problem, new findings, yet more questions, Development **132**, 2007 (2005).

[11] G. Britton, I. Heemskerk, R. Hodge, A. A. Qutub, and A. Warmflash, A novel self-organizing embryonic stem cell system reveals signaling logic underlying the patterning of human ectoderm, Development **146**, 179093 (2019).

[12] E. Karzbrun, A. H. Khankhel, H. C. Megale, S. M. K. Glasauer, Y. Wyle, G. Britton, A. Warmflash, K. S. Kosik, E. D. Siggia, B. I. Shraiman, and S. J. Streichan, Human neural tube morphogenesis in vitro by geometric constraints, Nature (London) **599**, 268 (2021).

[13] L. Wolpert, Positional information and the spatial pattern of cellular differentiation, J. Theor. Biol. **25**, 1 (1969).

[14] K. Dasbiswas, E. Hannezo, and N. S. Gov, Theory of epithelial cell shape transitions induced by mechanoactive chemical gradients, Biophys. J. **114**, 968 (2018).

[15] F. Brinkmann, M. Mercker, T. Richter, and A. Marciniak-Czochra, Post-Turing tissue pattern formation: Advent of mechanochemistry, PLoS Comput. Biol. **14**, e1006259 (2018).

[16] S. Okuda, T. Miura, Y. Inoue, T. Adachi, and M. Eiraku, Combining Turing and 3D vertex models reproduces autonomous multicellular morphogenesis with undulation, tubulation, and branching, Sci. Rep. **8**, 2386 (2018).

[17] P. Recho, A. Hallou, and E. Hannezo, Theory of mechanochemical patterning in biphasic biological tissues, Proc. Natl. Acad. Sci. USA **116**, 5344 (2019).

[18] J. S. Bois, F. Jülicher, and S. W. Grill, Pattern formation in active fluids, Phys. Rev. Lett. **106**, 028103 (2011).

[19] C. Parada, S. P. Banavar, P. Khalilian, S. Rigaud, A. Michaut, Y. Liu, D. M. Joshy, O. Campàs, and J. Gros, Mechanical feedback defines organizing centers to drive digit emergence, Dev. Cell **57**, 854 (2022).

[20] A. J. Engler, S. Sen, H. L. Sweeney, and D. E. Discher, Matrix elasticity directs stem cell lineage specification, Cell **126**, 677 (2006).

[21] E. Farge, Mechanical induction of twist in the drosophila foregut/stomodeal primordium, Curr. Biol. **13**, 1365 (2003).

[22] N. Desprat, W. Supatto, P.-A. Pouille, E. Beaurepaire, and E. Farge, Tissue deformation modulates twist expression to determine anterior midgut differentiation in drosophila embryos, Dev. Cell **15**, 470 (2008).

[23] G. F. Oster, J. D. Murray, and A. K. Harris, Mechanical aspects of mesenchymal morphogenesis, Development **78**, 83 (1983).

[24] A. E. Shyer, A. R. Rodrigues, G. G. Schroeder, E. Kassianidou, S. Kumar, and R. M. Harland, Emergent cellular self-organization and mechanosensation initiate follicle pattern in the avian skin, Science **357**, 811 (2017).

[25] K. H. Palmquist, S. F. Tiemann, F. L. Ezzeddine, S. Yang, C. R. Pfeifer, A. Erzberger, A. R. Rodrigues, and A. E. Shyer, Reciprocal cell-ECM dynamics generate supracellular fluidity underlying spontaneous follicle patterning, Cell **185**, 1960 (2022).

[26] T. R. Huycke, T. J. Häkkinen, H. Miyazaki, V. Srivastava, E. Barruet, C. S. McGinnis, A. Kalantari, J. Cornwall-Scoones, D. Vaka, Q. Zhu, H. Jo, R. Oria, V. M. Weaver, W. F. DeGrado, M. Thomson, K. Garikipati, D. Boffelli, O. D. Klein, and Z. J. Gartner, Patterning and folding of intestinal villi by active mesenchymal dewetting, Cell **187**, 3072 (2024).

[27] J. D. Murray and G. F. Oster, Generation of biological pattern and form, IMA J. Math. Appl. Med. Biol. **1**, 51 (1984).

[28] G. M. Odell, G. Oster, P. Alberch, and B. Burnside, The mechanical basis of morphogenesis. I. Epithelial folding and invagination, Dev. Biol. **85**, 446 (1981).

[29] X. Xue, Y. Sun, A. M. Resto-Irizarry, Y. Yuan, K. M. Aw Yong, Y. Zheng, S. Weng, Y. Shao, Y. Chai, L. Studer, and J. Fu, Mechanics-guided embryonic patterning of neuroectoderm tissue from human pluripotent stem cells, Nat. Mater. **17**, 633 (2018).

[30] S. M. Chambers, C. A. Fasano, E. P. Papapetrou, M. Tomishima, M. Sadelain, and L. Studer, Highly efficient neural conversion of human ES and iPS cells by dual inhibition of SMAD signaling, Nat. Biotechnol. **27**, 275 (2009).

[31] Y. Mica, G. Lee, S. M. Chambers, M. J. Tomishima, and L. Studer, Modeling neural crest induction, melanocyte specification, and disease-related pigmentation defects in hESCs and patient-specific iPSCs, Cell Rep. **3**, 1140 (2013).

[32] J. Tchieu, B. Zimmer, F. Fattahi, S. Amin, N. Zeltner, S. Chen, and L. Studer, A modular platform for differentiation of human PSCs into all major ectodermal lineages, Cell Stem Cell **21**, 399 (2017).

[33] I. Muñoz-Sanjuán and A. H. Brivanlou, Neural induction, the default model and embryonic stem cells, Nat. Rev. Neurosci. **3**, 271 (2002).

[34] E. Bier and E. M. De Robertis, BMP gradients: A paradigm for morphogen-mediated developmental patterning, Science **348**, aaa5838 (2015).

[35] S. Banerjee and M. C. Marchetti, Substrate rigidity deforms and polarizes active gels, Europhys. Lett. **96**, 28003 (2011).

[36] C. M. Edwards and U. S. Schwarz, Force localization in contracting cell layers, Phys. Rev. Lett. **107**, 128101 (2011).

[37] S. Banerjee and M. C. Marchetti, Contractile stresses in cohesive cell layers on finite-thickness substrates, Phys. Rev. Lett. **109**, 108101 (2012).

[38] M. Tewary, J. Ostblom, L. Prochazka, T. Zulueta-Coarasa, N. Shakiba, R. Fernandez-Gonzalez, and P. W. Zandstra, A stepwise model of reaction-diffusion and positional information governs self-organized human peri-gastrulation-like patterning, Development (Cambridge, England) **144**, 4298 (2017).

[39] F. Etoc, J. Metzger, A. Ruzo, C. Kirst, A. Yoney, M. Z. Ozair, A. H. Brivanlou, and E. D. Siggia, A balance between secreted inhibitors and edge sensing controls gastruloid self-organization, Dev. Cell **39**, 302 (2016).

[40] H. Nunley, X. Xue, Y. Sun, A. M. Resto-Irizarry, Y. Yuan, K. M. A. Yong, Y. Zheng, S. Weng, Y. Shao, D. K. Lubensky, L. Studer, and J. Fu, Dataset of cell layers on micro-patterned substrates composed of posts [Data set], University of Michigan - Deep Blue Data (2025), https://doi.org/10.7302/2kbj-1y73.

[41] J. Fu, Y.-K. Wang, M. T. Yang, R. A. Desai, X. Yu, Z. Liu, and C. S. Chen, Mechanical regulation of cell function with geometrically modulated elastomeric substrates, Nat. Methods **7**, 733 (2010).

[42] A. Saez, A. Buguin, P. Silberzan, and B. Ladoux, Is the mechanical activity of epithelial cells controlled by deformations or forces? Biophys. J. **89**, L52 (2005).

[43] Y. Sun, K. M. A. Yong, L. G. Villa-Diaz, X. Zhang, W. Chen, R. Philson, S. Weng, H. Xu, P. H. Krebsbach, and J. Fu, Hippo/YAP-mediated rigidity-dependent motor neuron differentiation of human pluripotent stem cells, Nat. Mater. **13**, 599 (2014).

[44] See Supplemental Material at http://link.aps.org/supplemental/10.1103/PhysRevResearch.7.L022051 for estimation of in-plane stress in colonies, estimation of cellular mechanical properties, simulations of tissue patterning on substrates of finite thickness, calculations based on the domain-wall approximation, and a more complete discussion of constraints on alternative models that rely on an unidentified chemical signal.

[45] F. Corson and E. D. Siggia, Geometry, epistasis, and developmental patterning, Proc. Natl. Acad. Sci. USA **109**, 5568 (2012).

[46] A. Raju and E. D. Siggia, A geometrical perspective on development, Dev. Growth Differ. **65**, 245 (2023),.

[47] M. Cross and H. Greenside, *Pattern Formation and Dynamics in Nonequilibrium Systems* (Cambridge University Press, Cambridge, 2009).

[48] E. Närvä, A. Stubb, C. Guzmán, M. Blomqvist, D. Balboa, M. Lerche, M. Saari, T. Otonkoski, and J. Ivaska, A strong contractile actin fence and large adhesions direct human pluripotent colony morphology and adhesion, Stem Cell Rep. **9**, 67 (2017).

[49] K. A. Rosowski, A. F. Mertz, S. Norcross, E. R. Dufresne, and V. Horsley, Edges of human embryonic stem cell colonies display distinct mechanical properties and differentiation potential, Sci. Rep. **5**, 14218 (2015).

[50] H. Nunley, X. Xue, J. Fu, and D. K. Lubensky, Dataset on cell areas and nuclear densities in differentiating stem cell colonies [Data set], University of Michigan - Deep Blue Data (2025), https://doi.org/10.7302/0n9v-6397.

[51] H. Nunley and D. K. Lubensky, Code for simulating the formation of a binary fate pattern in response to mechanical stresses [Data set], University of Michigan - Deep Blue Data (2025), https://doi.org/10.7302/44wm-j668.

[52] C. B. Muratov and S. Y. Shvartsman, An asymptotic study of the inductive pattern formation mechanism in Drosophila egg development, Physica D **186**, 93 (2003).

[53] C. B. Muratov and V. V. Osipov, General theory of instabilities for patterns with sharp interfaces in reaction-diffusion systems, Phys. Rev. E **53**, 3101 (1996).

[54] W. v. Saarloos, Three basic issues concerning interface dynamics in nonequilibrium pattern formation, Phys. Rep. **301**, 9 (1998).

[55] A. F. Mertz, Y. Che, S. Banerjee, J. M. Goldstein, K. A. Rosowski, S. F. Revilla, C. M. Niessen, M. C. Marchetti, E. R. Dufresne, and V. Horsley, Cadherin-based intercellular adhesions organize epithelial cell–matrix traction forces, Proc. Natl. Acad. Sci. USA **110**, 842 (2013).

[56] H. Nunley, X. Xue, Y. Sun, A. M. Resto-Irizarry, Y. Yuan, K. M. A. Yong, Y. Zheng, S. Weng, Y. Shao, D. K. Lubensky, L. Studer, and J. Fu, Dataset of stem cell colonies differentiating in neural induction medium and code for analysis of resulting fate pattern [Data set], University of Michigan - Deep Blue Data (2025), https://doi.org/10.7302/axdw-zm41.

[57] A. Saez, M. Ghibaudo, A. Buguin, P. Silberzan, and B. Ladoux, Rigidity-driven growth and migration of epithelial cells on microstructured anisotropic substrates, Proc. Natl. Acad. Sci. USA **104**, 8281 (2007).

[58] J. L. Tan, J. Tien, D. M. Pirone, D. S. Gray, K. Bhadriraju, and C. S. Chen, Cells lying on a bed of microneedles: An approach to isolate mechanical force, Proc. Natl. Acad. Sci. USA **100**, 1484 (2003).

[59] P. Caldarelli, A. Chamolly, A. Villedieu, O. Alegria-Prévot, C. Phan, J. Gros, and F. Corson, Self-organized tissue mechanics underlie embryonic regulation, Nature (London) **633**, 887 (2024).

[60] T. Das, K. Safferling, S. Rausch, N. Grabe, H. Boehm, and J. P. Spatz, A molecular mechanotransduction pathway regulates collective migration of epithelial cells, Nat. Cell Biol. **17**, 276 (2015).

[61] P. E. Farahani, S. B. Lemke, E. Dine, G. Uribe, J. E. Toettcher, and C. M. Nelson, Substratum stiffness regulates Erk signaling dynamics through receptor-level control, Cell Rep. **37**, 110181 (2021).

[62] I. Martyn, T. Y. Kanno, A. Ruzo, E. D. Siggia, and A. H. Brivanlou, Self-organization of a human organizer by combined Wnt and Nodal signalling, Nature (London) **558**, 132 (2018).

[63] H. Spemann and H. Mangold, Induction of embryonic primordia by implantation of organizers from a different species. 1923, Int. J. Dev. Biol. **45**, 13 (2001).

[64] P. Wilson, G. Lagna, A. Suzuki, and A. Hemmati-Brivanlou, Concentration-dependent patterning of the Xenopus ectoderm by BMP4 and its signal transducer Smad1, Development **124**, 3177 (1997).